Investigation of Li and H dynamics in Li_6C_{60} and $Li_6C_{60}H_y$ ✩

L. Maidich[a,*], D. Pontiroli[b], M. Gaboardi[b], S. Lenti[b], G. Magnani[b], G. Riva[b], P. Carretta[a], C. Milanese[c], A. Marini[c], M. Riccò[b], S. Sanna[a]

[a]*Dipartimento di Fisica, Università di Pavia, Via Bassi, 6, 27100 Pavia, Italy*
[b]*Dipartimento di Fisica e Scienze della Terra, Università di Parma, Viale delle Scienze, 7/a, 43124 Parma, Italy*
[c]*Pavia Hydrogen Lab, CSGI & Università di Pavia, Dipartimento di Chimica, Sezione di Chimica Fisica, Viale Taramelli, 16, 27100 Pavia, Italy*

Abstract

We report the extensive investigation of Li and H dynamics in Li_6C_{60} and $Li_6C_{60}H_y$, by combining ^{7}Li and ^{1}H solid state NMR measurements with DC/AC conductivity, in order to evaluate the potential application of these systems for energy-storage purposes. ^{7}Li NMR results show a local motion of Li ions above 200 K in both pristine and hydrogenated compounds, with activation energies of 90-150 meV and correlation times of about 30 ps. Evidences of Li interdiffusive dynamics are given by conductivity measurements in Li_6C_{60} already above 120 K, with activation energies of 240 meV, suggesting that ionic conductivity is of the order of 10^{-5} S·cm^{-1} at room temperature, with correlation times of about 150 ps. On the other hand, the $Li_6C_{60}H_y$ behaves like a semiconductor with a high energy gap (ca. 2.5 eV), suggesting that diffusion of intercalated Li ions is prevented. ^{1}H NMR measurements indicate the absence of H motions for the whole temperature range investigated (up to 360 K), neither on macroscopic or local scale. Li_6C_{60} good properties for H_2-storage are confirmed in terms of absorption capacity (5 wt% H_2), moreover we found that around 35% of lithium segregates in LiH form, leaving $Li_4C_{60}H_{40}$ as the final hydrogenation product.

1. Introduction

One of the major challenges of the current century is the exploitation of renewable and cleaner sources of energy to replace conventional fossil fuels. In particular, large efforts have been addressed to the identification of new materials able to improve the performances of solid-state energy-storage systems, such as components of Li-ion batteries, or solid state hydrogen-storage compounds. Recently, intercalated fullerides M_xC_{60} (M = alkali or alkaline-earth metal) has proven to be rather interesting for both these purposes [1, 2, 3, 4, 5, 6, 7, 8].

In these systems, the alkali ions usually occupy the tetrahedral and octahedral interstices of the *fcc* C_{60} network, forming charge-transfer salts. The relatively tight packing of the structure, induced by the Coulomb interaction among ions, tipically prevents the diffusion of alkali ions through the lattice. How-

---

ever, this rule can be overridden in the case of the smallest alkali or alkaline-earth ions, in particular Li and Mg. For instance, in Li_4C_{60} fullerenes polymerization takes place and leads to a monoclinic distortion of the parent *fcc* lattice, which seems to play a key role for enabling three-dimensional Li diffusion. As a result, this material displays a record Li-ion conductivity of 10^{-2} S/cm at room temperature, comparable to that observed in liquid electrolytes, with a relatively low activation energy,[2] and hence appears rather appealing as component in solid-state Li-ion batteries. Recently, a similar behaviour was also observed in the isostructural Mg_2C_{60}, where divalent Mg ion diffusion results in $0.5 \cdot 10^{-4}$ S/cm ion conductivity at room temperature, thus opening a new scenario on the possible development of new Mg ion batteries.[6] Despite these findings, to our knowledge only few studies on the possible applications of fullerides in Li-ion batteries have been made so far, which indeed have shown that C_{60}, both in the pure or the hydrogenated ($C_{60}H_y$) state, behaves as good negative electrode in Li-ion batteries, with potential capacity of up to 1200 mAh/g.[1] However, there is still much to understand about these systems. In particular, due to the known ability of solid C_{60} to intercalate high amount of Li atoms per molecule avoiding segregation,[9] it would be interesting to investigate Li ion properties in Li_xC_{60} also at the higher stiochiometries of Li, where fullerene polymerisation is prevented and Li form clusters in the C_{60} lattice interstices.[10, 11]

On the other hand, Li fullerides appeared suitable also for solid-state hydrogen storage applications. In particular, Li_6C_{60} is able to reversibly absorb up 5 wt% H_2 [4] at moderate thermodynamic conditions (onset at $\simeq$ 540 K), and up 5.9 wt% is reached when transition metal (Pt, Pd) small particles are added.[12] This represents a major improvement compared to pure C_{60}, where only 2.5 wt% H_2 is chemically absorbed at rather higher temperatures and irreversibly. The complex hydrogenation mechanism in Li fullerides was found to originate on the lithium clusters filling the octahedral interstices of the *fcc* C_{60} lattice, which first promote the H_2 dissociation[7] and then bring to the formation of the hydrofullerite. However, also in this case there are still some open questions. For example, the Li-H interaction seems to play a role in the reversibility of the Li_xC_{60} hydrogenation process, but it is not yet completely understood. At high Li doping level ($x = 12$), partial Li segregation in form of hydride was observed after hydrogenation,[5] but it is still not clear if this happens also in Li_6C_{60}. Since Li segregation is expected to change the anionic state of hydrogenated fullerene, thus affecting the thermodynamic stability of this molecule, its precise quantification could provide useful information on the physics of the desorption process.

In this manuscript, we report an extensive study of Li_6C_{60} and hydrogenated $Li_6C_{60}H_y$ in order to investigate the Li and H dynamics on both macroscopic and local scale. The combination of several different experimental techniques, such as solid state nuclear magnetic resonance spectroscopy (ssNMR), direct current (DC) and frequency dependent (AC) conductivity measurements, x-ray diffraction, thermogravimetry and calorimetry, allow us to explore the potentiality of this carbon nanostructure for energy storage purposes.

2. Experimental

About 300 mg of Li_6C_{60} powder has been synthesized following a previously reported procedure.[7] During the hydrogenation process, the powder was heated at 5 K/min from room temperature up to 623 K at 100 bar of hydrogen and appending a 10 h isotherm in a PCTPro-2000 manometric apparatus by Setaram & HyEnergy. 5.2 wt% hydrogen was absorbed at the end of the thermal/pressure treatment, in agreement with previous results.[4, 7] Powder X-ray diffraction (PXRD) analysis was performed by a Bruker D5005 diffractometer (Cu K_α radiation) in the angular range $2\theta = 5° - 50°$ by using a suitable, sealed zero-background sample holder, which allowed the measurements under oxygen- and moisture-free Ar atmosphere.

For the electric conductivity measurements, the samples have been prepared as cylindrical pellets of 4.5 mm diameter and 1 mm thickness. Pellets were sandwiched between either Li (non-blocking), or Fe (blocking) electrodes, which were then connected to the instrument by gold wire. In order to avoid oxygen and moisture contaminations, the cells were assembled in Ar glovebox (< 1 ppm O_2 and H_2O) and put in a suitable o-ring sealed sample-holder. Both DC and AC measurements were carried out in the temperature range $100 - 300$ K by means of an Oxford cryostat, operating with nitrogen flux. High temperature measurement in the range $300 - 520$ K were performed with a home-made furnace. DC conductivity measurements were performed with a Keithley 6221 current source and a Keithley 2182A nanovoltmeter, coupled in the Delta-mode configuration. AC conductivity measurements were per-

formed with a HP/Agilent 4192A LF impedance analyser in the frequency range between $5 - 5 \cdot 10^6$ Hz. AC conductivity measurements, the impedance was modeled with the Debye equivalent circuit (see the sketch put as inset in Figure 3), where a finite resistance R_i, which represents the ionic bulk resistance, is placed in series with the capacity C_{int} of the electrode/electrolyte interface; an additional capacity C_{geom}, in parallel with the previous elements, accounts of the bulk capacity dominating at high frequency.[13]

Nuclear magnetic resonance (NMR) measurements were carried out on a Tecmag Apollo spectrometer at applied magnetic fields of 1.5 T or 7.2 T. Both ^7Li and ^1H NMR spectra were performed by using a solid echo sequence of pulses ($\frac{\pi}{2} \rightarrow \tau_{echo} \rightarrow \frac{\pi}{2}$). Synthesized samples (50-80 mg) were sealed in NMR quality quartz vials and sealed under inert atmosphere. LiH (Aldrich, 95%) was used as received. A saturated solution of LiCl (Aldrich, $\geq 99\%$) was prepared as standard for the NMR measurements.

3. Results

3.1. X-ray diffraction

The structure of Li_6C_{60}, as shown by the PXRD analysis (Figure 1), shows a cubic *fcc* lattice similar to pristine C_{60} ($Fm\overline{3}m$ symmetry) with $a = 14.04(2)$ Å at RT, in agreement with literature data.[4] Li^+ ions are expected to occupy the interstitial sites of the cubic lattice, either the octahedral, Li_O ($\frac{1}{2}$ $\frac{1}{2}$ $\frac{1}{2}$), or the tetrahedral one Li_T ($\frac{1}{4}$ $\frac{1}{4}$ $\frac{1}{4}$). If these sites were fully occupied the stoichiometry would be Li_3C_{60}, therefore the larger octahedral site is expected to be occupied by four lithium
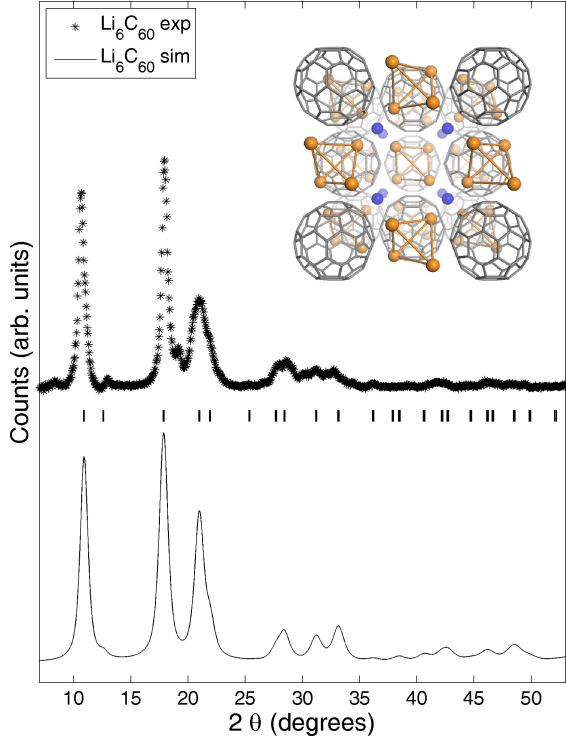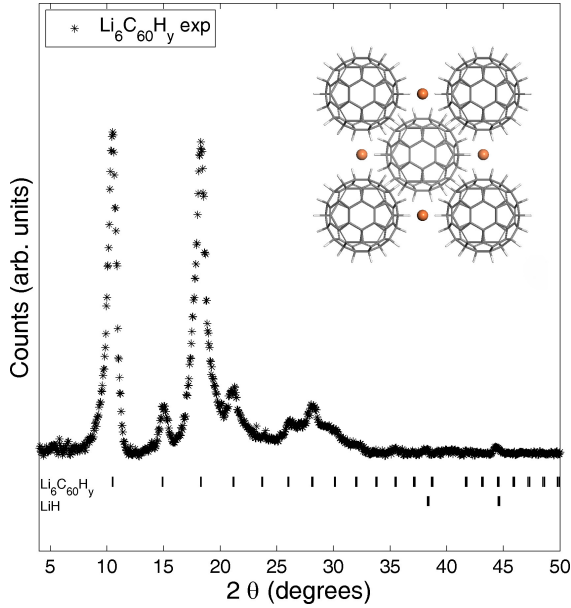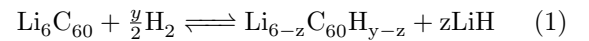
(a) Li_6C_{60}

(b) $Li_6C_{60}H_y$

Figure 1: Room temperature PXRD pattern of Li_6C_{60} and $Li_6C_{60}H_y$. Dotted line is the experimental diffraction pattern, while solid line shows the Li_6C_{60} calculated pattern from the suggested structure. The thick-marks represent the reflections positions according to the *bcc* structure of the cell. Insets: representation of the proposed crystal structures.

atoms, forming a cluster as suggested also by multiple quantum NMR measurements.[14] Although a detailed structural analysis was prevented, due to the low crystallinity of the sample and the resolution of the technique, it is reasonable to assume that the clusters in the octahedral site should have a conformation similar to Li arrangement observed in the high temperature phase of Li_4C_{60}.[15, 16] In that case, Li_O atoms were found to fully occupy the position 4b ($\frac{1}{2}$ $\frac{1}{2}$ $\frac{1}{2}$) and the remaining were disordered in the position 32f (x x x) of the $Fm\bar{3}m$ C_{60} cell with $x = 0.375$. It makes sense to assume here that the disordered 32f site is able to host more alkali atoms, in order to satisfy the Li_6C_{60} stoichiometry. It is worth noting here that in Li_6C_{60} PXRD pattern some weak and broad peaks were also detected, indexed as a minor fraction of the polymeric Li_4C_{60} phase.

The Li intercalated fullerane $Li_6C_{60}H_y$ crystallizes in a cubic *bcc* lattice, similarly to $C_{60}H_{36}$, with a lattice constant of $a = 11.85(2)$ Å (see Figure 1b). The rearrangement of the structure from *fcc* to *bcc* after hydrogenation could be rationalised by the loss of icosahedral symmetry in the $C_{60}H_y$ molecule.[17] The PXRD pattern also shows the presence of weak peaks, indexed as the LiH phase. However, the estimation of the relative amounts of the two phases was not possible in this case, due to the absence of a precise structural model for Li intercalated fullerane.

The presence of LiH in the hydrogenated sample suggests the following hydrogenation path:
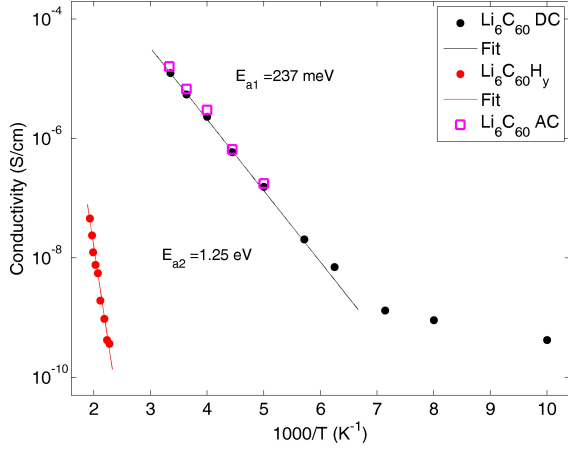
$$Li_6C_{60} + \frac{y}{2}H_2 \rightleftharpoons Li_{6-z}C_{60}H_{y-z} + zLiH \quad (1)$$

4

Figure 2: Li_6C_{60} DC conductivity values in the range $100 - 300$ K (black dots). The temperature dependence shows an activated behaviour for $T > 150$ K and, when fitted by the Arrhenius law (black line), an activation energy of 237 meV was calculated. DC conductivity of $Li_6C_{60}H_y$ in the $440 - 520$ K range (red dots). Data fitted by the Arrhenius model (red line) showed a high-gap semiconducting behaviour.

If we assume $z = 0$, on the basis of manometric measurements we can evaluate the maximum stoichiometry after hydrogenation as $Li_6C_{60}H_{42}$. In order to simplify the discussion, from now on, we will refer to the hydrogenated Li_6C_{60} as $Li_6C_{60}H_y$ (taking into account that only equation 1 describes reasonably the products of hydrogenation).

3.2. Conductivity

DC conductivity measurements performed on Li_6C_{60} show two distinct regimes (see Figure 2, black dots). At low temperatures ($T < 150$ K), the conductivity is almost temperature independent with a very low value of about 10^{-9} S·cm^{-1}. On the other hand, for $T > 150$ K, it increases with temperature with an activated behavior, up to $\sim 10^{-5}$ S·cm^{-1} value at RT. The observed behaviour, qual-
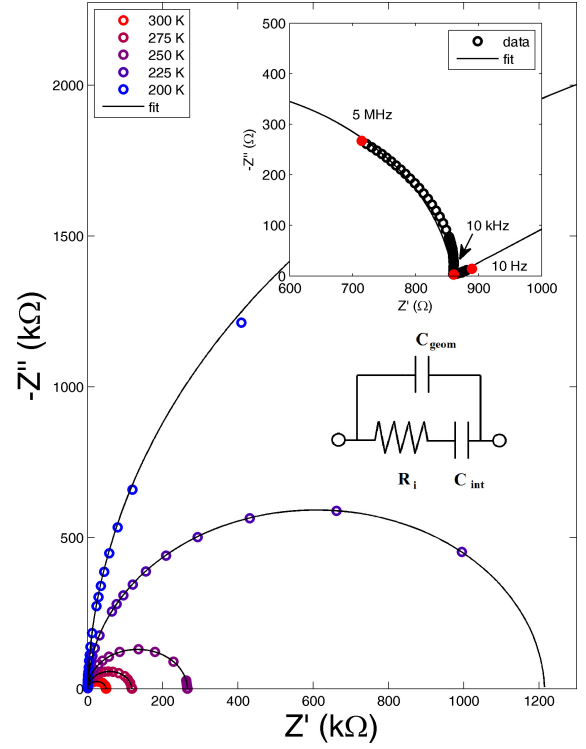

Figure 3: Cole-Cole diagrams of the impedance data of Li_6C_{60} measured in the range $200 - 300$ K in non-blocking configuration (open circles). Data were fitted by the Debye model, provided that the capacity C_{int} of the equivalent circuit is equal to zero. Inset: Cole-Cole diagram at $T = 283$ K measured on Li_6C_{60} in the blocking configuration (open black circles). Data were fitted according to the Debye model (solid black line).

itatively similar to that of Li_4C_{60}, suggests the onset of a ionic contribution to the conductivity at $T \sim 150$ K, due to the Li ion diffusion in the sample. The linear range in the semilogarithmic plot was fitted by the Arrhenius law, leading to an activation energy, E_a^{DC}, of nearly 240 meV, similar to that observed in the superionic conductor Li_4C_{60}.[2] In order to deeply investigate the ionic nature of this compound, AC conductivity experiment was performed on Li_6C_{60}, by measuring the complex impedance of the sample, either with the non-blocking, or with the blocking configuration. In presence of an ionic conductor, these two measurements are expected to provide significantly different results, since in the former case the capacity of the electrode/electrolyte interface is negligible and hardly measurable (Li ions can move freely across the interface), while in the latter it should have a well definite value.

In Figure 3, the Cole-Cole diagrams in the complex impedance plane are shown for the AC conductivity measurements of Li_6C_{60} in the non-blocking configuration. The curves appear as single semi-circles terminating in the origin, and can be fitted by means of the Debye circuit discussed in the Experimental Section, provided that the capacity C_{int} is equal to zero, as expected (corresponding to the simple parallel combination of bulk resistance and bulk capacity). The fit of the arcs allowed us to extract the values of R_i and C_{geom} at the different temperatures; the formers are in very good agreement with the DC data (see Figure 2, magenta squares), while the latters were almost independent from T and fall in the typical range of tens of pF.
In the inset of Figure 3 AC conductivity measure-

ment performed on Li_6C_{60} in the blocking configuration at 283 K is displayed. In this case, the curve in the Cole-Cole diagram consists of a semi-arc with a small straight tail that forms an angle of about $45°$ with the real axis. This feature is commonly observed in ionic conductors, this being due to the ionic charge accumulation at the blocking electrode/electrolytes interfaces, and gives a further proof of the ionic behaviour of Li_6C_{60}. The high frequency circle expected in the Cole-Cole diagram cannot be completed in the experimental frequency window, but the fit of the data by means of the De-bye circuit (solid black line, inset Figure 3) shows that this is expected to terminate in the origin for sufficiently high probing frequencies. The observed slope for the low-frequency tail is another common feature in the complex impedance plots of solid electrolytes and can be rationalised by taking into account the spurious processes occurring at the solid electrolyte/electrode interface.[18] Similar features were observed in the AC conductivity data in the temperature range $253 - 343$ K.

The rationale behind this result is that for Li_6C_{60} the activated behaviour observed in DC measurements has to be ascribed mainly to the ionic contribution of Li ions to diffusion, while the electronic contribution is expected to be negligible, its value being close to that measured at low temperatures ($T < 150$ K).

DC measurements at RT on a pellet of $Li_6C_{60}H_y$ indicated that the sample has a resistance greater than 1 GΩ, therefore, it can be considered as an insulator at this temperature, both from an electronic and ionic point of view. At higher temperatures, between $440 - 520$ K, the conductivity data display
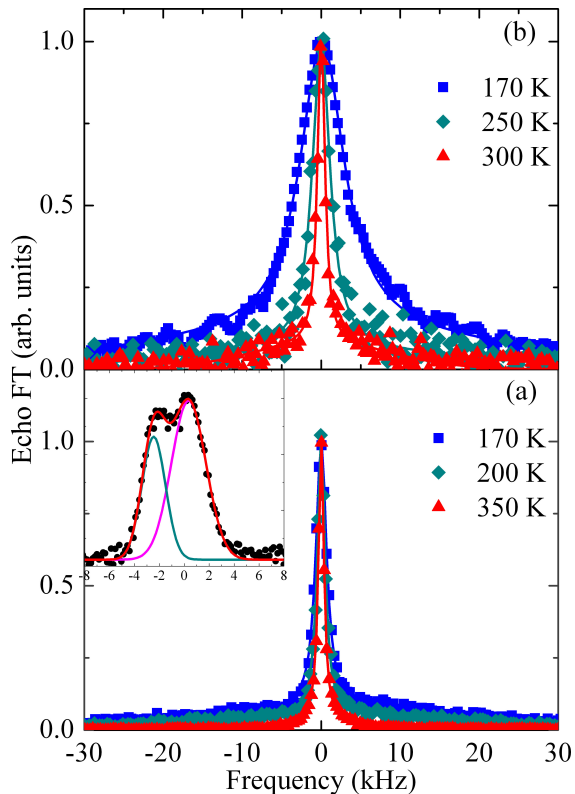
Figure 4: (a) ^{7}Li NMR spectra of Li_6C_{60} and $Li_6C_{60}H_y$ (b) as measured at different temperatures. The lines are the best fit either to a sum of two Gaussian or Lorentzian peaks (see text). Inset: Li_6C_{60} spectrum at $T = 67$ K.

a semiconducting behaviour and the measured gap is 2.5 eV (see Figure 2, red dots and red solid line). It was not possible to perform impedance measurements due to the high resistance of the sample.

3.3. ^7Li NMR Spectroscopy

^{7}Li NMR static spectra of Li_6C_{60} and $Li_6C_{60}H_y$ are displayed in Figure 4. The data in the temperature range $100 - 200$ K can be fitted by the sum of two Gaussian contributions: a narrow line, assigned to $\frac{1}{2} \leftrightarrow -\frac{1}{2}$ central transition, and a broad line, assigned to the $\pm\frac{3}{2} \leftrightarrow \pm\frac{1}{2}$ satellite transition, in agreement with previous results.[14] The observation that the length of the $\frac{\pi}{2}$ NMR pulse is the
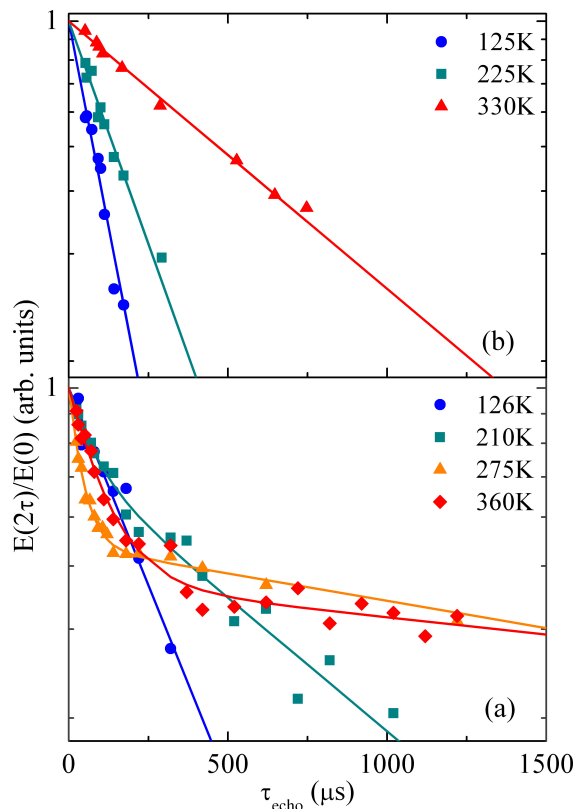

Figure 5: ^{7}Li echo decay as a function of the time τ_{echo} between the two $\frac{\pi}{2}$ pulses for (a) Li_6C_{60} and (b) $Li_6C_{60}H_y$. The lines are the best fit either to a single or a double exponential decay rate (see text).

same of a saturated LiCl reference solution confirms that both the central and the satellite lines were fully irradiated. The corresponding linewidths are $\Delta\nu_{\frac{1}{2},-\frac{1}{2}} = 2$ and 6 kHz and $\Delta\nu_{\pm\frac{3}{2},\pm\frac{1}{2}} = 35$ and 40 kHz for Li_6C_{60} and $Li_6C_{60}H_y$, respectively. Since the broadening of the central line is mainly due to nuclear dipolar couplings, a larger $\Delta\nu$ is expected in the hydrogenated sample, where an additional hetero-dipolar interaction between ^1H and ^7Li magnetic moments is present. In both samples the lineshape changes from Gaussian to Lorentzian as the temperature is increased above 200 K and the linewidth tightens.

The observed narrowing upon heating points towards the onset of low-frequency dynamics, which modulates the local field at the ^7Li nuclei. In fact, when the time scale of the fluctuations, characterized by a correlation time τ_c, becomes shorter than the inverse of the low-temperature frequency distribution $\Delta\omega_0$, the motional narrowing of the NMR spectrum is attained.[19] As already observed in previous works,[14, 16] this narrowing can be associated to the activated motion of Li ions. In the inset of Figure 6 the temperature dependence of the narrower component ($\Delta\nu_{\frac{1}{2},-\frac{1}{2}}$) is shown for both of the investigated compounds. The two displayed linewidths confirm again the presence of a motional narrowing effect in both samples Li_6C_{60} and $Li_6C_{60}H_y$.

In the case of Li_6C_{60}, the central line at the lowest temperature attained, $T = 67$ K, splits in two peaks as shown in the inset of Figure 4a. In this case from the fit of the two lines the spectrum intensity ratio is about 2:1. This result reflects the presence of two inequivalent lithium sites, namely the tetrahedral and the octahedral ones. A very similar behaviour was previously observed in the ^{23}Na NMR of Na_6C_{60}, where the two observed lines collapse into one at much higher temperature showing only one line above 400 K.[20] This temperature difference is due to the much lower mobility of Na compared to that of Li ions.

In order to further study the dynamics, the spin-spin (T_2) and spin-lattice (T_1) relaxation times were measured as a function of temperature. Figure 5 displays the echo amplitude as a function of the time delay between the first $\frac{\pi}{2}$ pulse and the echo signal, τ_{echo}, obtained by a quadrupolar echo $\frac{\pi}{2} - \tau - \frac{\pi}{2}$ pulse sequence, for Li_6C_{60} and $Li_6C_{60}H_y$ samples. The curves have been fitted according to a general two-component exponential function

$$y = A \exp\left(-\frac{2\tau_{echo}}{T_{2a}}\right) + B \exp\left(-\frac{2\tau_{echo}}{T_{2b}}\right)$$

which describes the presence of two different local environments for ^7Li nuclei, with a slow ($T_{2a} \approx 200 - 1000$ μs) and a fast ($T_{2b} < 30$ μs) relaxation time respectively. The latter is clearly observed above ~ 150 K only for the pure Li_6C_{60}, while it is wiped out in all the other measurements. This fast component indicates the presence of a rather high local dipolar field at the resonant nucleus and suggests that a fraction of the Li ions forms a tight cluster, in agreement with what observed in multiple quantum NMR measurements. [14] From a comparison with a LiH reference sample we estimate a missing fraction of 50% in both the pure and hydrogenated compounds at 300 K (see below).

The $\frac{1}{T_{2a}}$ as a function of the inverse temperature of Li_6C_{60} and $Li_6C_{60}H_y$ is shown in Figure 6. At high temperature the data can be fitted to an Arrhenius

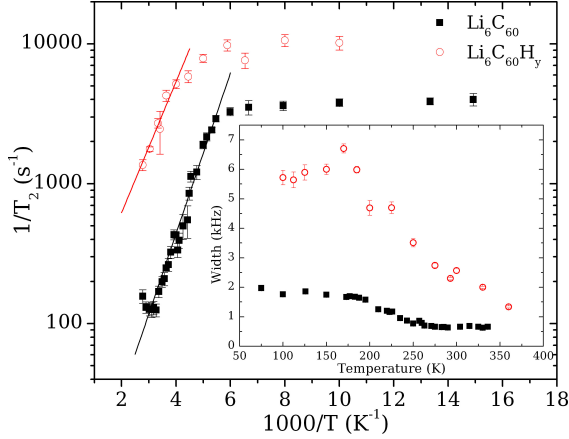Figure 6: ^{7}Li $\frac{1}{T_2}$ *vs* $\frac{1000}{T}$ and $\Delta\nu$ *vs* T (inset) for Li_6C_{60} and $Li_6C_{60}H_y$. The lines are the best fit to an Arrenius behaviour for $T \gtrsim 200$ K.

Figure 7: ^{7}Li recovered magnetization curves of Li_6C_{60}, $Li_6C_{60}H_y$ and LiH at RT and $\mu_0 H = 7.2$ T. The solid lines are the best fit curves (see text).

law which reflects a thermally activated behaviour. The best fit provides the activation energy of the process as $E_a^{T_2} \sim 100$ meV for both the samples.

The spin-lattice relaxation time T_1 has been measured using a standard saturation recovery pulse sequence. Figure 7 shows the recovery of the nuclear magnetization as a function of the delay between the saturating and the readout pulses, at RT and $\mu_0 H = 7.2$ T, both for the pure and hydrogenated Li_6C_{60}. For comparison, the recovery of the LiH reference sample is also shown. The Li_6C_{60} points can be fitted by the following recovery law:

$$M_z = M_\infty \left(1 - \exp\left(-\frac{t}{T_1} \right)^\beta \right)$$

where $T_1 \sim 100$ ms and a stretching coefficient $\beta \simeq 0.9$ was found at room temperature. On the other hand, the $Li_6C_{60}H_y$ curve requires the sum of two components, one with a relaxation time similar to the one of Li_6C_{60}, $T_{1a} \sim 1.5$ ms, and an additional one of about $T_{1b} \sim 8500$ s ($\beta_a \approx 1$ and $\beta_b = 0.75$), and relative amplitudes $M_{\infty,a} = 0.15$
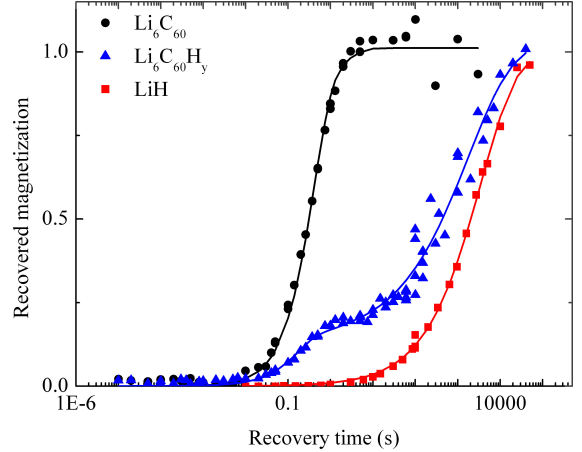
and $M_{\infty,b} = 0.85$.

The detection of two very different spin-lattice relaxation rates in $Li_6C_{60}H_y$ indicates the presence of two distinct ^{7}Li species, one comparable to that observed in Li_6C_{60} and a second one with a much longer T_1, very close to the one measured in the LiH reference sample. The former component is likely to be due to those lithium ions still intercalated in the hydrofullerite structure. This implies that hydrofullerene is found in its anionic state $C_{60}H_{y-z}^{n-}$. The difference in the T_1 of the second component is due to the fact that the segregated LiH experiences a different local environment compared to that of a pure LiH phase. This is likely to be caused by the fact that the LiH, originated from the segregation of lithium from $Li_6C_{60}H_y$, is nanostructured thus yielding to particles sufficiently large to be detected by X-ray diffraction (see above) but not enough to reproduce the bulk LiH phase environment.

The presence of LiH is in agreement with previous results on higher stoichiometry compounds showing
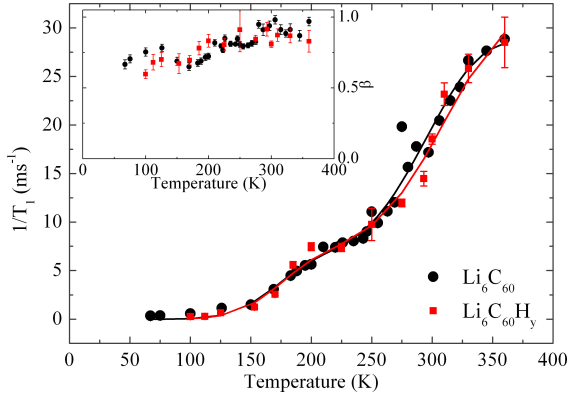
Figure 8: ^{7}Li $\frac{1}{T_1}$ vs T for Li$_6$C$_{60}$ and Li$_6$C$_{60}$H$_y$ at $\mu_0 H = 1.5$ T. Solid lines are the results of the BPP fit (see text). The inset shows the temperature behavior of the related stretched coefficient β.

that hydrogenation of alkali fullerides leads to the formation of alkali hydride,[21, 3, 8, 11]. From the relative amplitudes $M_{\infty,a}$ and $M_{\infty,b}$ and by considering the missing fraction of 50%, one can roughly estimate that about 35% of Li nuclei are present in LiH form. This allows us to rewrite the equation 1 as following:

$$\mathrm{Li_6C_{60} + 21H_2 \rightleftharpoons Li_4C_{60}H_{40} + 2LiH} \quad (2)$$
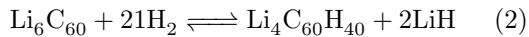
We note that the hydrofullerene anion stoichiometry is not far from that of C$_{60}$H$_{36}$, considered one of the most stable neutral hydrogenated compounds of C$_{60}$.[22]

Figure 8 shows ^{7}Li $\frac{1}{T_1}$ (1/T_{1a} for the hydrogenated sample) vs T, at $\mu_0 H = 1.5$ T, for Li$_6$C$_{60}$ and Li$_6$C$_{60}$H$_y$. The inset shows the temperature dependence of the related stretching coefficient β. In the investigated range, i.e. $100 \div 360$ K, the samples display an almost overlapping trend suggesting that the spin-lattice relaxation rate is negligibly affected by the presence of hydrogen and
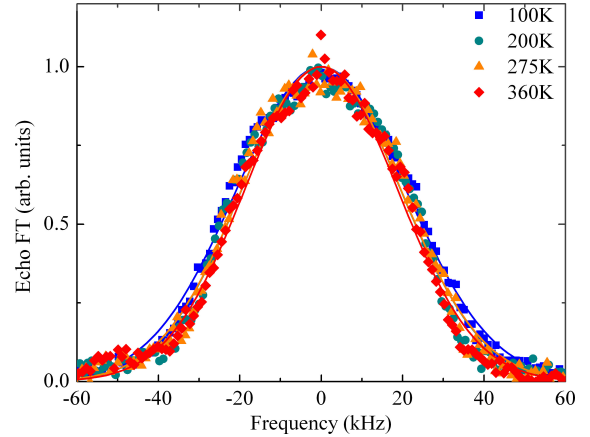

Figure 9: ^{1}H NMR spectra recorded at different temperatures for Li$_6$C$_{60}$H$_y$ at $\mu_0 H = 1.5$ T.

probably mainly affected by the cluster internal dynamics.

The observed behaviour can be fitted according to a sum of two BPP functions[23] for a dipolar relaxation mechanism with two different thermally activated relaxation times generally described as $\tau_i = \tau_{c,i} \exp\left(\frac{E_{a,i}^{T_1}}{T}\right)$:

$$\frac{1}{T_1} \approx \sum_{i=1,2} \frac{D_i \tau_i}{1 + \omega_L^2 \tau_i^2} + \frac{4 D_i \tau_i}{1 + 4\omega_L^2 \tau_i^2}$$

where D_i is a constant, $E_{a,i}^{T_1}$ (i=1,2) is the activation energy associated to the process and ω_L is the ^{7}Li Larmor frequency. The extracted values for $E_{a,i}^{T_1}$ and the correlation times ($\tau_{c,1} \approx \tau_{c,2} \sim 30$ ps) are reported in Table 1.

3.4. ^{1}H NMR Spectroscopy of Li$_6$C$_{60}$H$_y$

Li$_6$C$_{60}$H$_y$ was studied also by means of ^{1}H NMR, in order to further investigate the microscopic dynamics. In Figure 9 we show the NMR spectra at $\mu_0 H = 1.5$ T at different temperatures. The
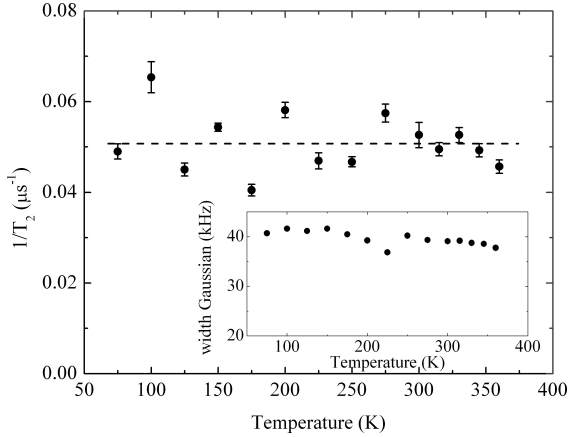
10

Figure 10: $\frac{1}{T_2}$ vs T for $Li_6C_{60}H_y$. In the inset is shown $\Delta\nu$ vs T.
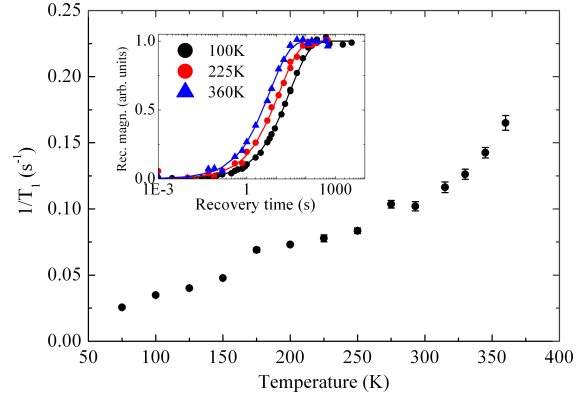

Figure 11: $\frac{1}{T_1}$ obtained for different temperatures. Inset: [1]H recovery curves as a function of the repetition time for different temperatures.

spectra can be fitted according to a single Gaussian function and their linewidth is almost temperature independent with a value of $\sigma \approx 40$ kHz (see inset in Figure 10).

Measurements of the spin-spin relaxation time of the ^{1}H nuclei have been analyzed with a single exponential decay function over the entire range of temperature. The $\frac{1}{T_2}$ values thus obtained oscillate around a constant average value that can be estimated as $T_2 \approx 20 \pm 3$ μs^{-1}, as shown of Figure 10, in agreement with the constant linewidth.

The T_1 of the ^{1}H nuclei has been measured by means of a standard saturation recovery pulse sequence and the recovery of the nuclear magnetization fits to a stretched exponential $M_z = M_\infty \left(1 - \exp\left(-\frac{T}{T_1}\right)^\beta\right)$, with $\beta \simeq 0.65$ over the whole T range (inset of Figure 11). This indicates a distribution of relaxation rates associated to the different local environments probed by the ^{1}H nuclei.

The temperature dependence of $\frac{1}{T_1}$ relaxation rate is shown in Figure 11. It resembles those obtained for [7]Li in Figure 8, suggesting that the [1]H T_1 is mainly affected by the Li ionic dynamics and confirming that no significant H motion occurs up to $T = 360$ K.

From the comparison between the intensities of the ^{1}H NMR echoes of $Li_6C_{60}H_y$ and that of a calibrated reference water solution at room temperature we can estimate that the amount of stored H content is 5.0 ± 0.5 wt%, in agreement with the manometric measurements reported above.

4. Discussion

The combination of the different experimental techniques employed in this study allows us to investigate the dynamics of Li in Li_6C_{60} and of Li and H in $Li_6C_{60}H_y$, with the aim to consider the potential of this carbon nanostructures for energy-storage applications. Concerning the use of these materials as components in lithium-ion batteries, the most important insights come from the combination of the ^{7}Li NMR and the AC/DC conductivity measurements. The former has

11

Table 1: Comparison between activation energies (in meV units) and correlation times (in ps) as obtained in this work from T_2 and/or T_1 NMR and AC/DC conductivity measurements.

Sample	$E_a^{T_2}$	$E_{a1}^{T_1}$	$E_{a2}^{T_1}$	E_a^{DC}	E_a^{AC}	$\tau_c^{T_1}$	τ_c^{AC}
$\mathrm{Li_6C_{60}}$	110 ± 10	90 ± 10	150 ± 10	240 ± 40	240 ± 30	~ 30	~ 150
$\mathrm{Li_6C_{60}H_y}$	90 ± 10	90 ± 10	150 ± 10	-	-	~ 30	-

demonstrated that both $\mathrm{Li_6C_{60}}$ and the hydrogenated samples display a narrowing of the $^7\mathrm{Li}$ NMR spectra at high temperatures, which is thermally activated above 200 K (inset of Figure 6). This motional narrowing can be related to the motion of the $\mathrm{Li^+}$ interstitial ions. This dynamics is further confirmed by the temperature dependence of the T_2 spin-spin relaxation time. In fact, the analysis of the $\frac{1}{T_2}(\mathrm{T})$ behavior in Figure 6 highlights the presence of a thermally activated process, with an activation energy of about 100 meV. The thermal activation of the Li motions is also supported by the study of the T_1 spin-lattice relaxation time as a function of temperature (Figure 8), which clearly shows two distinct dynamics (whose energy barriers are displayed in Table 1) and a similar correlation time, $\tau_c^{T_1} \approx 30$ ps, as explained in Section 3.3. This behavior suggests that two inequivalent interstitial sites are populated by lithium, which are compatible with the presence of either tetrahedral or octahedral interstitial sites in the *fcc* lattice. An additional Li clustering is suggested by the behaviour of one of the two component, showing a fast T_2 decay rate, which yields to the loss of nearly 50% of the $^7\mathrm{Li}$ NMR signal, as explained in Section 3.3. This is in good agreement with the hydrogenation mechanism previously hypothesized.[7]
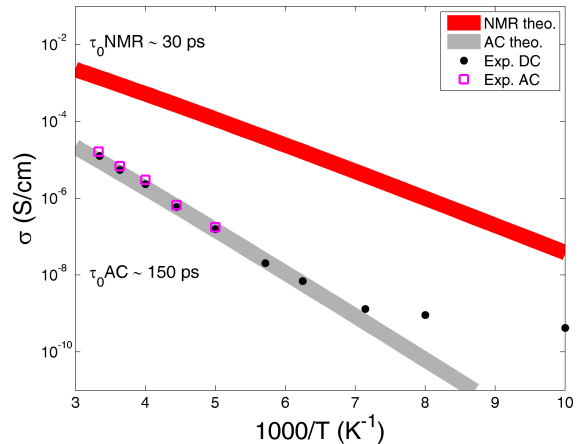

Figure 12: Temperature dependence of the electrical conductivity of $\mathrm{Li_6C_{60}}$ as extracted from DC/AC data (black dots and magenta open squares respectively) and calculated from the Nernst-Einstein model described by equation 3 with $^7\mathrm{Li}$ NMR parameters (red thick line). The grey thick line shows the calculated electrical conductivity assuming $\tau_0 \sim 150$ ps.

Despite the fact that $^7\mathrm{Li}$ NMR shows that the Li motion does occur both in $\mathrm{Li_6C_{60}}$ and $\mathrm{Li_6C_{60}H_y}$, only the former presents a sizeable ionic conductivity, as shown by AC/DC conductivity measurements. A rough estimation of the correlation times involved in the Li ion diffusion in $\mathrm{Li_6C_{60}}$ can be obtained by comparing the experimental electrical conductivity with the one estimated by the Nernst-Einstein equation, in the hypothesis of simple hopping model, neglecting correlation effects:

$$\sigma = \frac{Nl^2(Ze)^2}{2n\tau k_B T} \tag{3}$$

12

where N is the number of charge carriers per volume ($\sim 9.45 \cdot 10^{21}$ cm^{-3}), l is the hopping distance (Li$_O$-Li$_T$ distance of 3.04 Å), Ze is the electrical charge of the carrier, n is a dimensional factor ($n = 1,2,3$, respectively for one-, two- and three dimensional diffusion), τ is the correlation time, assumed to have an Arrhenius temperature dependence. In Figure 12 the measured temperature dependence of DC/AC electrical conductivity (respectively black dots and magenta open squares) is plotted together with that evaluated from the ^{7}Li NMR parameters using equation 3 (red thick line).

It turns out that both the correlation time and the activation energy determined from the BPP fit of the $T_1(T)$ behaviour (Figure 8) would account for a ionic conductivity of two order of magnitude greater than the measured one, which on the contrary seems to be compatible with an hopping process with larger time-scales, of the order of 150 ps (grey thick line). Since local jumps are expected to be faster than those of the intersite diffusion, this fact suggests that the ^{7}Li NMR signal of Li$_6$C$_{60}$ is mainly dominated by the local Li$^+$ motions between the nearest next neighbors interstitial sites, while the conductivity measurements can only detect the intersite migration throughout the whole sample.

In addition, the activation energies as determined from the analysis of the temperature dependece of the T_1 and T_2 relaxation rates, are lower on average than those evaluated by the conductivity measurements, as summarized in Table 1. In fact, the activation of the local motions may require less energy than the intersite diffusion.

The AC/DC conductivity measurements indicate that Li$_6$C$_{60}$ behaves as an ionic conductor with a room temperature conductivity of the order of 10^{-5} S·cm^{-1}. This value is lower than the one measured in Li$_4$C$_{60}$, but still interesting for applications (for comparison, ionic conductivity of Li-intercalated graphite[24] is of the same order of magnitude). The observed differences are probably due to the structural differences between the two compounds: Li$_4$C$_{60}$ is a 2D polymer crystal, where the fullerenes are linked by covalent bonds, while the Li$_6$C$_{60}$ has a monomer *fcc* structure, similar to that of C$_{60}$. The size of the tunnels connecting the tetrahedral and octahedral interstitial sites, where Li ions are intercalated in the two materials, are different and this might cause the difference in the observed conductivity values. Noteworthy, the ionic conductivity is almost completely inhibited after hydrogenation.

The NMR data show that the hydrogenation process yields to the formation of a sizeable quantity of LiH and that the amount of interstitial Li$^+$ is then reduced to $\sim 65\%$ of the total amount, corresponding to 4 lithium ions still held in the hydrofulleride interstices. Furthermore, the hydrogenation of C$_{60}$ molecule leads to an increase of the steric hindrance thus yielding to a structural rearrangement of molecules to a *bcc* configuration. The interplay between these two effects easily interrupts the conductive channels, thus totally preventing the ion migration of the residual interstitial Li$^+$ in Li$_6$C$_{60}$H$_y$. The electronic contribution to the conductivity is also very low, less than that observed in the pure C$_{60}$, as the HOMO electrons, previously contributing to the electronic conductivity, are now involved into the covalent bonding with H. These findings on hydrogenated Li$_6$C$_{60}$ seem to partially contradict

the results found by Loutfi et al., which suggested that both Li intercalated C_{60} and hydrogenated C_{60} would be good electrodes for Li-ion batteries.[25] As far as the solid state hydrogen-storage applications are concerned both manometric and NMR investigations show that about 5 wt% H_2 is stored in Li_6C_{60},[7, 4] and additionally most of it is bound to C_{60} forming $C_{60}H_{40}$ anion in $Li_4C_{60}H_{40}$, while the remaining hydrogen is bound to segregated Li in form of hydride. The charged state of $C_{60}H_{40}$ decreases the energy requested to start the dehydrogenation process, since the transferred electrons are likely to populate the anti-bonding orbitals of the molecule, lastly yielding to a lower desorption temperature. Both the almost temperature independent ^{1}H NMR linewidth and T_2 measurements (Figure 10) indicate the absence of H motions for $T < 360$ K neither on macroscopic or local scale that is in agreement with the formation of strong C-H bonds between fullerene and the incoming hydrogen. This behavior is quite different to that recently observed in defective graphene, where ^{1}H NMR evidenced a diffusive dynamics of the hydrogens chemically bound to graphene sheets already above 200 K, with a correlation time of a few microseconds.[26]

The absence of any dynamics involving hydrogen nuclei in $Li_6C_{60}H_y$ suggests that, in the investigated temperature range, the system is still far to affect C-H bonds stability in the intercalated hydrofullerene.

5. Conclusions

In this work we carried out an extensive investigation of the Li and H dynamics on both macroscopic and local scale of Li_6C_{60} and $Li_6C_{60}H_y$ compounds with the aim to further investigate the capability of these carbon nanostructures for energy storage purposes.

With respect to the potentiality as H_2-storage system, we confirmed 5.2 wt% H_2 absorption capability and we suggest the formation of $Li_4C_{60}H_{40}$ as the final stoichiometry for the hydrogenation process. The presence of Li ions intercalated in the hydrofullerene structure is considered to be the most important ingredient to lower the energy barrier necessary to release the chemisorbed hydrogen.

The ^{1}H NMR investigation showed that the motion of hydrogen is inhibited for the whole investigated temperature range $70 - 360$ K, even on the local scale indicating that the C-H bonds are still rather strong near room temperature.

On the other hand, the study of the ^{7}Li NMR shows a local scale dynamics between the nearest next neighbors Li ions in both Li_6C_{60} and $Li_6C_{60}H_y$, characterized by an activation energy in the range of $90 - 150$ meV and correlation times $\tau_c^{T_1}$ of the order of 30 ps, in two distinct interstitial sites (possibly the tetrahedral and octahedral ones present in the *fcc* lattice). Complete AC/DC conductivity measurements show a sizeable intersite ion migration in the Li_6C_{60} sample, with an activation energy of ~240 meV and an estimated τ_c^{AC} ~150 ps. Noteworthy, the room temperature ionic conductivity is of the order of 10^{-5} S·cm^{-1}. Even if this value is much lower than the one measured in

Li_4C_{60}, it is comparable with that of Li-intercalated graphite,[24] making this compound interesting as possible component in lithium-ion batteries. On the other hand, the hydrogenated fulleride behaves like a semiconductor, with a high energy gap (~ 2.5 eV), indicating that the Li ion diffusion is prevented in this case. In fact, it is found that the hydrogenation reduces the quantity of the interstitial lithium, which partially forms LiH and also induces a strong deformation of the former fullerene-like structure, possibly closing the conductive channels.

Acknowledgements

References

[1] R. Loutfy, S. Katagiri, Fullerene materials for lithium-ion battery applications, in: E. Ōsawa (Ed.), Perspectives of Fullerene Nanotechnology, Springer Netherlands, 2002, pp. 357–367. doi:10.1007/0-306-47621-5_32.
URL http://dx.doi.org/10.1007/0-306-47621-5_32

[2] M. Riccò, M. Belli, M. Mazzani, D. Pontiroli, D. Quintavalle, A. Jánossy, G. Csányi, Superionic conductivity in the li4c60 fulleride polymer, Phys. Rev. Lett. 102 (2009) 145901. doi:10.1103/PhysRevLett.102.145901.
URL http://link.aps.org/doi/10.1103/PhysRevLett.102.145901

[3] P. Mauron, A. Remhof, A. Bliersbach, A. Borgschulte, A. Züttel, D. Sheptyakov, M. Gaboardi, M. Choucair, D. Pontiroli, M. Aramini, A. Gorreri, M. Riccò, Reversible hydrogen absorption in sodium intercalated fullerenes, International Journal of Hydrogen Energy 37 (19) (2012) 14307 – 14314, {HYFUSEN} Special Issue for the 4th National

- 3rd Latin American Conference on Hydrogen and Sustainable Energy Sources (HYFUSEN), 6-9 June 2011, Mar Del Plata, Argentina. doi:http://dx.doi.org/10.1016/j.ijhydene.2012.07.045.
URL http://www.sciencedirect.com/science/article/pii/S0360319912016229

[4] J. A. Teprovich, M. S. Wellons, R. Lascola, S.-J. Hwang, P. A. Ward, R. N. Compton, R. Zidan, Synthesis and characterization of a lithium-doped fullerane (lix-c60-hy) for reversible hydrogen storage, Nano Letters 12 (2) (2012) 582–589, pMID: 22206302. arXiv:http://dx.doi.org/10.1021/nl203045v, doi:10.1021/nl203045v.
URL http://dx.doi.org/10.1021/nl203045v

[5] P. Mauron, M. Gaboardi, A. Remhof, A. Bliersbach, D. Sheptyakov, M. Aramini, G. Vlahopoulou, F. Giglio, D. Pontiroli, M. Riccò, A. Züttel, Hydrogen sorption in li12c60, The Journal of Physical Chemistry C 117 (44) (2013) 22598–22602. arXiv:http://dx.doi.org/10.1021/jp408652t, doi:10.1021/jp408652t.
URL http://dx.doi.org/10.1021/jp408652t

[6] D. Pontiroli, M. Aramini, M. Gaboardi, M. Mazzani, A. Gorreri, M. Riccò, I. Margiolaki, D. Sheptyakov, Ionic conductivity in the mg intercalated fullerene polymer mg2c60, Carbon 51 (0) (2013) 143 – 147. doi:http://dx.doi.org/10.1016/j.carbon.2012.08.022.
URL http://www.sciencedirect.com/science/article/pii/S0008622312006744

[7] M. Aramini, M. Gaboardi, G. Vlahopoulou, D. Pontiroli, C. Cavallari, C. Milanese, M. Riccò, Muon spin relaxation reveals the hydrogen storage mechanism in light alkali metal fullerides, Carbon 67 (0) (2014) 92 – 97. doi:http://dx.doi.org/10.1016/j.carbon.2013.09.063.
URL http://www.sciencedirect.com/science/article/pii/S0008622313009172

[8] P. Mauron, M. Gaboardi, D. Pontiroli, A. Remhof, M. Riccò, A. Züttel, Hydrogen desorption kinetics in metal intercalated fullerides, The Journal of Physical Chemistry C 119 (4) (2015) 1714–1719. arXiv:http://dx.doi.org/10.1021/jp511102y, doi:10.1021/jp511102y.
URL http://dx.doi.org/10.1021/jp511102y

[9] M. Yasukawa, S. Yamanaka, Synthesis of

lixc60(x=1–28) fullerides under high-pressure and high-temperature conditions and their electrical properties, Chemical Physics Letters 341 (5–6) (2001) 467 – 475. `doi:http://dx.doi.org/10.1016/S0009-2614(01)00544-9`.
URL `http://www.sciencedirect.com/science/article/pii/S0009261401005449`

[10] F. Giglio, D. Pontiroli, M. Gaboardi, M. Aramini, C. Cavallari, M. Brunelli, P. Galinetto, C. Milanese, M. Riccò, Li12c60: A lithium clusters intercalated fulleride, Chemical Physics Letters 609 (0) (2014) 155 – 160. `doi:http://dx.doi.org/10.1016/j.cplett.2014.06.036`.
URL `http://www.sciencedirect.com/science/article/pii/S0009261414005417`

[11] M. Gaboardi, C. Cavallari, G. Magnani, D. Pontiroli, S. Rols, M. Riccò, Hydrogen storage mechanism and lithium dynamics in li12c60 investigated by μsr, Carbon 90 (0) (2015) 130 – 137. `doi:http://dx.doi.org/10.1016/j.carbon.2015.03.072`.
URL `http://www.sciencedirect.com/science/article/pii/S0008622315002808`

[12] M. Aramini, C. Milanese, D. Pontiroli, M. Gaboardi, A. Girella, G. Bertoni, M. Riccò, Addition of transition metals to lithium intercalated fullerides enhances hydrogen storage properties, International Journal of Hydrogen Energy 39 (5) (2014) 2124 – 2131. `doi:http://dx.doi.org/10.1016/j.ijhydene.2013.11.087`.
URL `http://www.sciencedirect.com/science/article/pii/S0360319913028504`

[13] R. Huggins, Simple method to determine electronic and ionic components of the conductivity in mixed conductors a review, Ionics 8 (3-4) (2002) 300–313. `doi:10.1007/BF02376083`.
URL `http://dx.doi.org/10.1007/BF02376083`

[14] M. Tomaselli, B. H. Meier, M. Riccò, T. Shiroka, A. Sartori, A multiple-quantum nuclear magnetic resonance study of interstitial li clusters in li_xc_{60}, The Journal of Chemical Physics 115 (1) (2001) 472–476. `doi:http://dx.doi.org/10.1063/1.1377014`.
URL `http://scitation.aip.org/content/aip/journal/jcp/115/1/10.1063/1.1377014`

[15] M. Riccò, M. Belli, D. Pontiroli, M. Mazzani, T. Shiroka, D. Arčon, A. Zorko, S. Margadonna, G. Ruani, Recovering metallicity in A_4c_{60}: The case of monomeric li_4c_{60}, Phys. Rev. B 75 (2007) 081401. `doi:10.1103/PhysRevB.75.081401`.
URL `http://link.aps.org/doi/10.1103/PhysRevB.75.081401`

[16] D. Arčon, A. Zorko, M. Mazzani, M. Belli, D. Pontiroli, M. Riccò, S. Margadonna, The structural and electronic evolution of li_4c_{60} through the polymer–monomer transformation, New Journal of Physics 10 (3) (2008) 033021.
URL `http://stacks.iop.org/1367-2630/10/i=3/a=033021`

[17] F. Cataldo, S. Iglesias-Groth (Eds.), Fulleranes: The Hydrogenated Fullerenes, Springer Netherlands, 2010. `doi:10.1007/978-1-4020-9887-1`.

[18] I. D. Raistrick, C. Ho, R. A. Huggins, Ionic conductivity of some lithium silicates and aluminosilicates, Journal of The Electrochemical Society 123 (10) (1976) 1469–1476. `arXiv:http://jes.ecsdl.org/content/123/10/1469.full.pdf+html`, `doi:10.1149/1.2132621`.
URL `http://jes.ecsdl.org/content/123/10/1469.abstract`

[19] A. Abragam, The Principles of Nuclear Magnetism, International series of monographs on physics, Clarendon Press, 1961.
URL `http://books.google.it/books?id=dyJRAAAAMAAJ`

[20] F. Rachdi, L. Hajji, M. Galtier, T. Yildirim, J. E. Fischer, C. Goze, M. Mehring, ^{13}C and ^{23}Na nmr studies of na_2c_{60} and na_6c_{60} fullerides, Phys. Rev. B 56 (1997) 7831–7834. `doi:10.1103/PhysRevB.56.7831`.
URL `http://link.aps.org/doi/10.1103/PhysRevB.56.7831`

[21] A. Yoshida, T. Okuyama, T. Terada, S. Naito, Reversible hydrogen storage/release phenomena on lithium fulleride (linc60) and their mechanistic investigation by solid-state nmr spectroscopy, J. Mater. Chem. 21 (2011) 9480–9482. `doi:10.1039/C1JM11542A`.
URL `http://dx.doi.org/10.1039/C1JM11542A`

[22] P. A. Cahill, Hydrogenated Fullerenes, World Scientific Publishing Co. Pte. Ltd., 1995, Ch. 4, pp. 53–66. `arXiv:http://www.worldscientific.com/`

doi/pdf/10.1142/9789812386250_0004, doi:10.1142/
9789812386250_0004.
URL http://www.worldscientific.com/doi/abs/10.
1142/9789812386250_0004

[23] N. Bloembergen, E. M. Purcell, R. V. Pound, Relax-
ation effects in nuclear magnetic resonance absorption,
Phys. Rev. 73 (1948) 679–712. doi:10.1103/PhysRev.
73.679.
URL http://link.aps.org/doi/10.1103/PhysRev.73.
679

[24] M. Park, X. Zhang, M. Chung, G. B. Less,
A. M. Sastry, A review of conduction phe-
nomena in li-ion batteries, Journal of Power
Sources 195 (24) (2010) 7904 – 7929. doi:http:
//dx.doi.org/10.1016/j.jpowsour.2010.06.060.
URL http://www.sciencedirect.com/science/
article/pii/S0378775310010463

[25] R. Loutfy, S. Katagiri, Fullerene materials for lithium-
ion battery applications, in: E. Ōsawa (Ed.),
Perspectives of Fullerene Nanotechnology, Springer
Netherlands, 2002, pp. 357–367. doi:10.1007/
0-306-47621-5_32.
URL http://dx.doi.org/10.1007/0-306-47621-5_32

[26] D. Pontiroli, M. Aramini, M. Gaboardi, M. Maz-
zani, S. Sanna, F. Caracciolo, P. Carretta, C. Cav-
allari, S. Rols, R. Tatti, L. Aversa, R. Verucchi,
M. Riccò, Tracking the hydrogen motion in defec-
tive graphene, The Journal of Physical Chemistry C
118 (13) (2014) 7110–7116. arXiv:http://dx.doi.org/
10.1021/jp408339m, doi:10.1021/jp408339m.
URL http://dx.doi.org/10.1021/jp408339m